Asian Journal of Chemistry; Vol. 35, No. 9 (2023), 2203-2209

ASIAN JOURNAL OF CHEMISTRY

https://doi.org/10.14233/ajchem.2023.28099

Effect of H_2O_2 Concentration on Morphology, Reflectivity and Wettability of Silicon Nanowalls Prepared by Metal Assisted Chemical Etching

ANIL KUMAR BEHERA[1,2], R.N. VISWANATH[3,*] and TOM MATHEWS[1]

[1]Surface and Nanoscience Division, Materials Science Group, Indira Gandhi Centre for Atomic Research, Homi Bhabha National Institute, Kalpakkam-603102, India
[2]Department of Physics, Government Autonomous College, Angul-759143, India
[3]Centre for Nanotechnology Research, Department of Humanities and Science, Aarupadai Veedu Institute of Technology, Vinayaka Mission's Research Foundation (DU), Chennai-603104, India

*Corresponding author: E-mail: rnviswanath@avit.ac.in

Received: 4 June 2023; *Accepted*: 25 July 2023; *Published online*: 31 August 2023; AJC-21365

A facile and low cost method, metal assisted chemical etching was used to prepare silicon (Si) nanowalls atop the Si wafer, where the effect of etchant solution concentration (H_2O_2 concentration) on the morphology, reflectivity and wettability of the fabricated Si nanowalls is investigated. The morphological and structural studies by scanning and transmission electron microscopy revealed the Si nanowalls prepared at both low and high H_2O_2 concentration are smooth, nonporous and single crystalline, where the increase of H_2O_2 concentration only changes the morphology from isolated nanowall structure to agglomerated nanowall structure. The height of nanowalls also increases with increase in H_2O_2 concentration and follows a linear behaviour with an etching rate of 5697 nm/M. The reflectance study shows that the reflectance is extremely low over broad wavelength range (300-1100 nm) for Si nanowalls, compared to that of planar Si wafer. The increase of H_2O_2 concentration significantly changes the wavelength dependence of the reflectance spectrum. The wettability studies show that SiNWs prepared at low H_2O_2 concentration exhibit hydrophobicity in contrast to the hydrophilicity of planar Si wafer, where the increase of H_2O_2 concentration to very high value changes the hydrophobicity of SiNWs to hydrophilicity as similar to planar Si wafer.

Keywords: Silicon nanowalls, Metal assisted chemical etching, Morphology, Reflectivity, Wettability.

INTRODUCTION

Semiconductor nanostructures have been attracting a great deal of scientific attention in fundamental research and technological applications because they exhibit exciting physical and chemical properties and possess excellent size dependent materials properties [1,2]. In particular, silicon (Si) nanostructures are being explored intensively in diverse fields such as electronics, photonics, photovoltaic, field emission devices, X-ray optics, medicine, energy storage, biosensors [3-7]. Numerous techniques like vapour-liquid-solid (VLS) growth, molecular beam epitaxy, laser ablation, *etc.* under the bottom-up approach category and reactive ion etching, laser-induced etching, electrochemical etching (or anodic polarization etching) and metal assisted chemical etching (MACE), *etc.* under the top-down approach category have been developed for the fabrication of Si nanostructures [8,9].

Among them, MACE has been the focus of extensive scientific and technological attention in the recent past because of the following reasons [3,10-12]. (i) It is a facile, room temperature and cost-effective technique wherein almost all procedures can be carried out in a chemical lab without needing any expensive equipment; (ii) It has the ability to produce different kind of nanostructures such as nanopores, nanowires, nanowalls and porous nanowires/nanowalls *etc.*, (iii) it is capable of controlling cross-sectional shape, size, length, orientation, *etc.* of fabricating nanostructures.

In recent years, silicon nanostructures prepared by MACE are found to exhibit extremely low light reflectance in a wide wavelength range [13-16]. Because of its extremely low reflectance, the silicon nanostructures appear as black in colour on compared to that of the grey metallic luster appearance of planar silicon. The high surface area black coloured silicon produced by MACE has been utilized for a wide range of applications

This is an open access journal, and articles are distributed under the terms of the Attribution 4.0 International (CC BY 4.0) License. This license lets others distribute, remix, tweak, and build upon your work, even commercially, as long as they credit the author for the original creation. You must give appropriate credit, provide a link to the license, and indicate if changes were made.

including fabrication of photodetectors, antireflection coating for silicon solar cells, micro-electro mechanical devices, light-emitting devices, image sensors, biochemical sensors, lithium-ion batteries, hydrogen production through water splitting, antibacterial coatings, a supporting medium for chemical and physical reactions, *etc.* [13,16-21].

It offers several advantages over the conventional anti-reflection coatings, for example, it gives extensively lower reflectance in broad spectral range, free from issues related to lattice mismatch, adhesiveness, stability and also leads to the reduction in cost for mass production. Additionally, black silicon synthesized by MACE is found to exhibit hydrophobic/super-hydrophobic behaviour, which is useful for not only increasing their efficiency, but also improving the life-time of solar cells [14,22,23]. However, the existence of dual behaviours *i.e.* the extremely low reflectance (black nature) and hydrophobicity are highly dependent on the morphology of fabricated nanostructures, which in turn depends on the etching parameters. So, in the present study, the effect of the most important etching parameter, H_2O_2 concentration on the morphology, reflectivity and wettability of metal assisted synthesized Si nanostructures is investigated.

EXPERIMENTAL

P-type (boron doped), single crystalline (100)-oriented, 1-10 Ω cm resistivity Si wafers (500 µm thick) were used for MACE to produce Si nanostructures. Prior to etching, the wafers were ultrasonically cleaned with deionized water (18.2 MΩ cm), acetone and ethanol for 15 min, followed by copious rinsing with deionized water. Subsequently, the Si wafers were immersed into freshly prepared piranha solution (3:1 ratio of 98% H_2SO_4 and 30% H_2O_2) to remove the residual organic contaminants and washed thoroughly with deionized water. Then, the wafers were dipped in dilute HF solution to remove the surface oxide layer, rinsed thoroughly with deionized water and finally dried with dry N_2 gas purging.

The Si wafer were then housed into the home made Teflon electrochemical cell as described earlier [10] and the etching (two-step MACE) was carried out successfully, where only one side of the Si wafer was in contact with the etching solution. In first step, silver (Ag) deposition was carried out using a solution of HF and $AgNO_3$ (5% HF + 0.02 M $AgNO_3$) for 60 s. In second step, etching was carried out using a solution of fixed HCl concentration (4.8 M HF) with various concentrations of H_2O_2 (0.2, 0.4, 0.6, 0.8 and 1 M H_2O_2) for 10 min. Each step was followed by rinsing with the deionized water. Finally, the etched Si wafer was immersed in conc. HNO_3 solution to obtain silver-free Si nanostructures, washed thoroughly with deionized water and kept them in vacuum desiccators for further investigations.

The Si etching was carried out at room temperature in dark condition. It is important to observed that only one side of the Si wafer was in contact with the etching solution in cell, hence the Si nanostructures formed only on that side. The morphology and microstructures of fabricated Si nanostructures were studied using a scanning electron microscope (SEM; Zeiss-Supra 55), Park XE7 atomic force microscope (AFM) and LIBRA 200FE Zeiss high resolution transmission electron microscope (HRTEM). The reflectivity and wettability studies were carried out using a commercial UV-Vis-NIR spectrophotometer (Hitachi UH4150) and Kruss makedrop shape analyzer DSA100, respectively.

RESULTS AND DISCUSSION

Morphological studies: Fig. 1 summarizes the SEM results of Si wafer etched in 4.8 M HF at 0.2, 0.4, 0.6, 0.8 and 1 M H_2O_2 concentrations. Figs. 1a-e and Fig. 1f-j illustrate their top and cross-sectional SEM micrograph views, respectively. As evident from the morphology, the surface relief Si nanostructures grown a top to the Si wafer etched at lowest H_2O_2 concentration (0.2 M) were found to be vertical, whereas at higher H_2O_2 concentrations, the surface relief Si nanostructures agglomerated at their top regions.

Fig. 2a-c depict high magnified SEM images of the top, middle and bottom part of Si wafer etched in 1 M H_2O_2, respectively. The red-arrow in Fig. 2c identifies the broken nanostructure. As evidenced from the morphology of the broken Si nanostructures, the surface relief Si nanostructures are in wall-like shape of thickness in the range between 70 and 80 nm. Fig. 1k shows height variation of SiNWs as a function of H_2O_2 concentrations and it was observed that the SiNWs height varies linearly with H_2O_2 concentration with an etching rate of 5697 nm/M. This observation is in close agreement with that reported by Moumni & Jaballah [24], where a nonlinear height dependence on H_2O_2 concentration with attenuation of height at higher H_2O_2 concentrations is demonstrated.

Fig. 2d shows the TEM image of a typical nanowall. It reveals that the wall surface is smooth and free of pores, which is in support of the cross-section SEM results (Fig. 1). Fig. 2e displays the HRTEM image of the wall structure, which represent that the etched Si walls are single crystalline in nature. The analysis of the HRTEM image gives an interplanar distance of 3.2 ± 0.1 Å, which corresponds to interplanar distance of the Si (111) [International Centre for Diffraction data, File: 00-005-0565]. Therefore, the fabricated surface relief Si nanostructures are hereafter denoted as silicon nanowalls (SiNWs). Here, in MACE, the variation in H_2O_2 concentration changes the surface morphology from isolated Si nanowall structures to agglomerated Si nanowalls structures. The effect of variation of H_2O_2 concentration on the morphology of fabricated Si nanostructures was also studied by Liu *et al.* [25], where they have reported that there is a change in the morphology from planar nanowires to porous structured nanowires with the variation in H_2O_2 concentration.

Fig. 3 illustrates the AFM topographic images of 1 M H_2O_2 etched Si wafer taken in different observation areas, 30 × 30 μm^2, 10 × 10 μm^2, 5 × 5 μm^2 and 2 × 2 μm^2. It is seen from the AFM micrographs that the morphology of SiNWs is uniform throughout the etched region. The image analysis further confirmed that the surface topography of the resulting etched Si nanowalls is close to that of SEM results. The qualitative agreement of the topography and the characteristic feature size of the etched Si further confirmed that the surface relief Si nanostructures evolved were in the shape of walls.

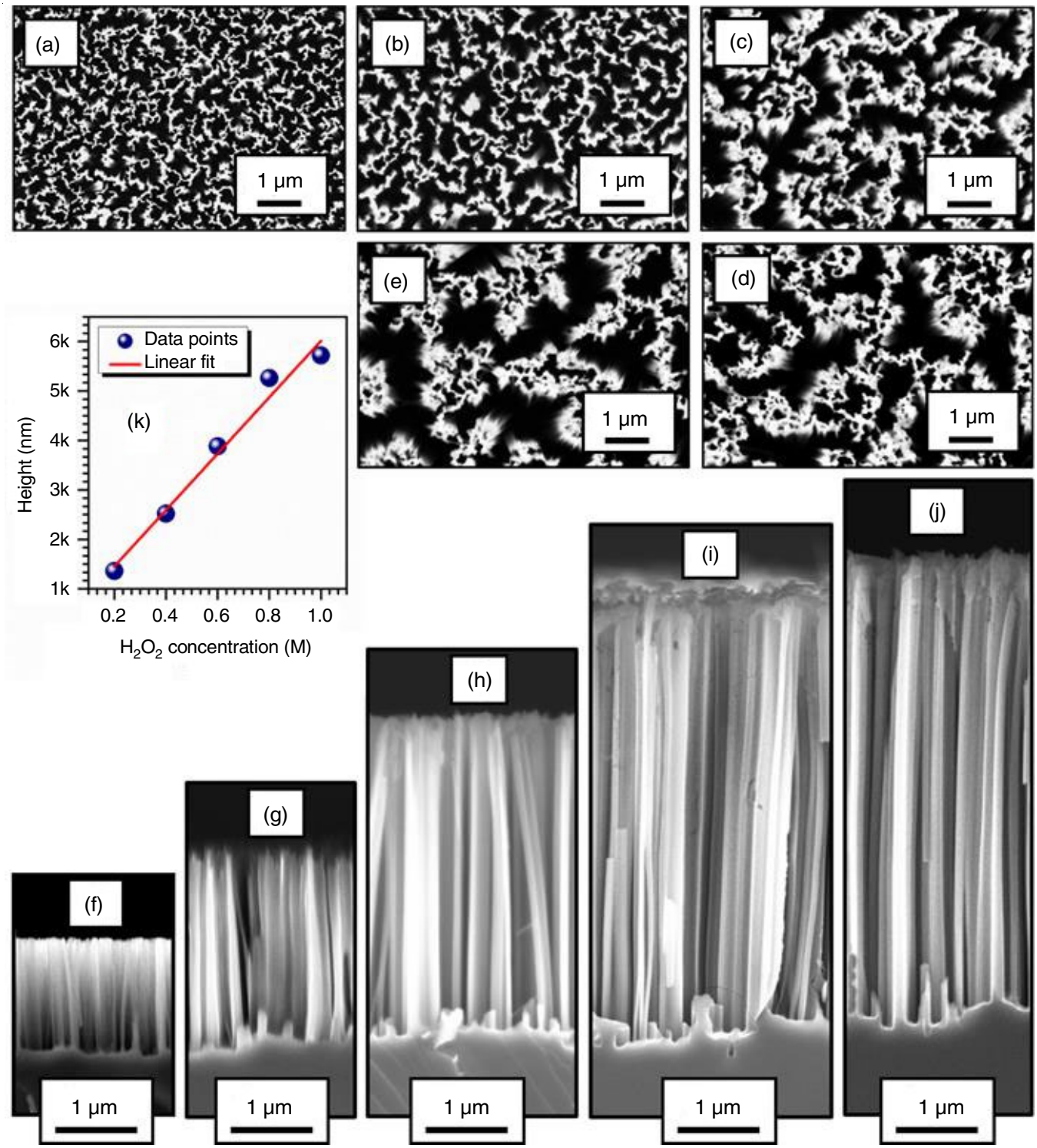

Fig. 1. Scanning electron micrographs of (100) oriented Si wafer etched in 4.8 M HF with different H_2O_2 concentrations for 10 min etching time. (a-e) and (f-j) depicts the top and cross-sectional view SEM images of sample obtained at 0.2, 0.4, 0.6, 0.8 and 1 M H_2O_2 concentration. (k) Illustrates the height of fabricated nanostructures *vs.* H_2O_2 concentration. The straight line (red colour) in sub figure (k) shows a linear fit to the data points (blue colour), with an etching rate (slope) of 5697 nm/M

The morphological behaviour of fabricated nanowall formations as a function of H_2O_2 concentration requires further investigation of the underlying etching mechanisms. The possible etching mechanisms for the formation of SiNWs by two steps MACE were discussed elaborately in the literature [7,14,26]. Therefore, the useful redox reaction involving the etching of Si wafer can be summarized as:

At cathode:

$$H_2O_2 + 2H^+ + 2e^- \longrightarrow 2H_2O \quad (1)$$

At anode:

$$Si + 2H_2O \longrightarrow SiO_2 + 4H^+ + 4e^- \quad (2)$$

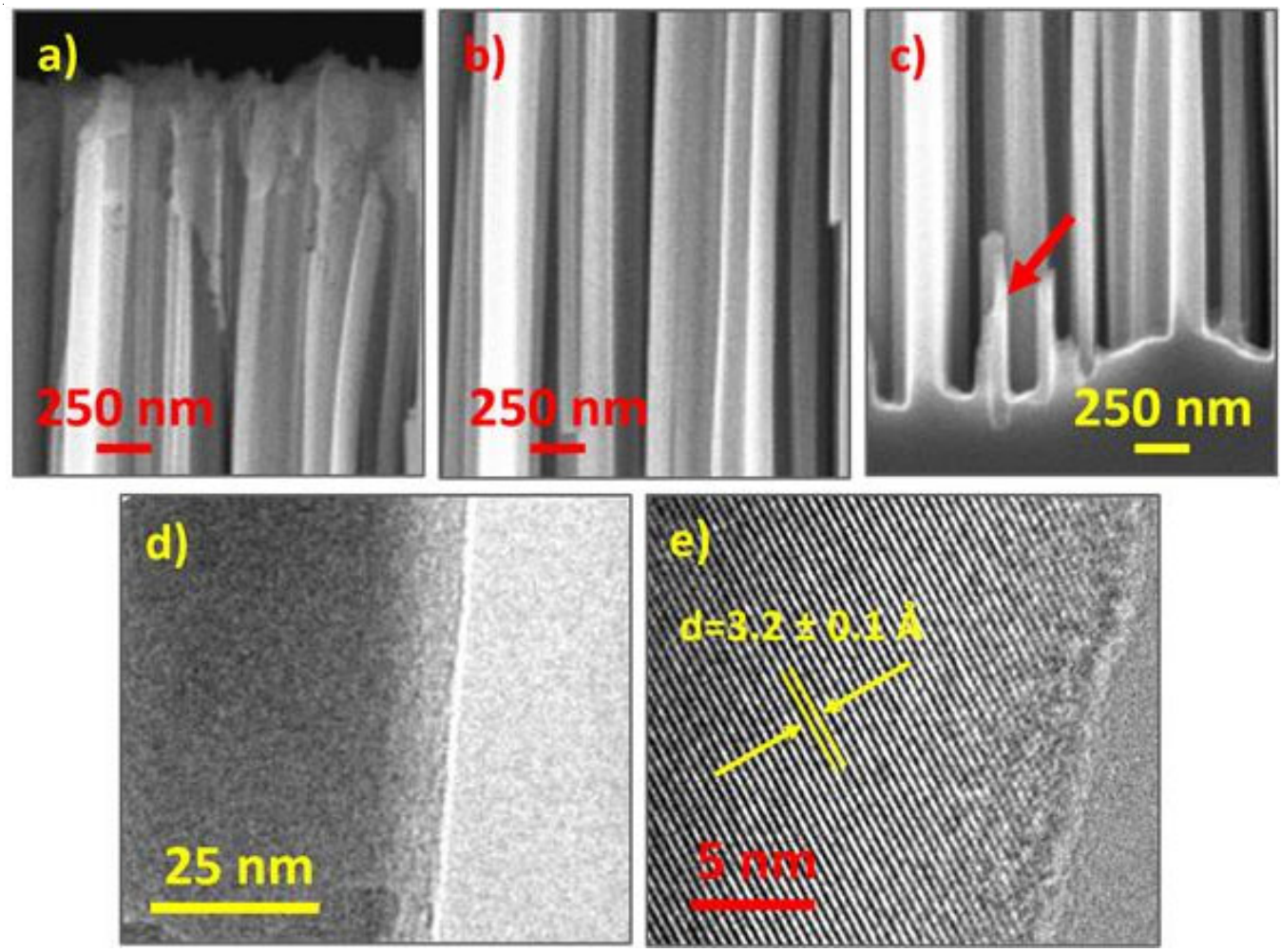

Fig. 2. (a-c) High magnification SEM images of top, middle and bottom part of Si wafer prepared at 1 M H_2O_2. (d) Typical TEM image of a nanowall. (e) HRTEM image of a selected region in Fig. (d). The image analysis gives inter-planar Si (111) distance of 3.2 ± 0.1 Å

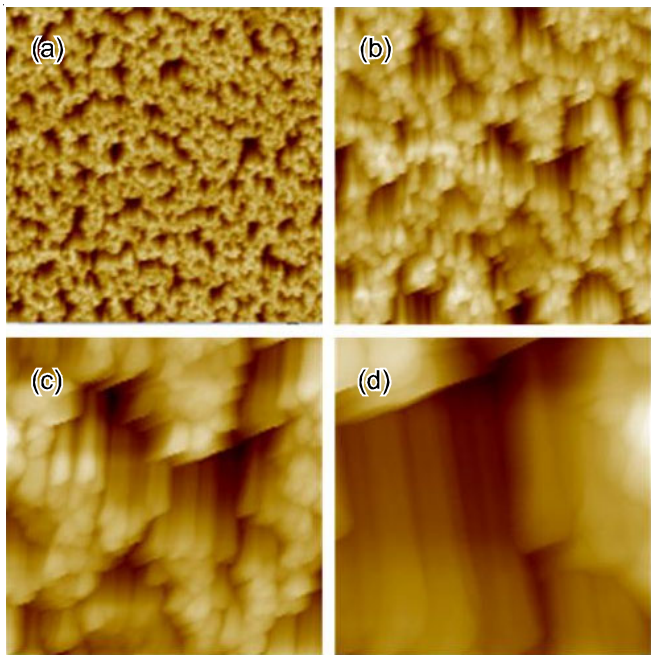

Fig. 3. AFM images of surface relief Si nanowall structures evolved on 1 M H_2O_2 etched Si wafer taken in different observation areas (a) 30 × 30 μm^2, (b) 10 × 10 μm^2, (c) 5 × 5 μm^2 and (d) 2 × 2 μm^2

$$SiO_2 + 6HF \longrightarrow [SiF_6]^{2-} + 2H_2O + 2H^+ \quad (3)$$

Total reaction:

$$Si + 2H_2O_2 + 6F^- + 4H^+ \longrightarrow [SiF_6]^{2-} + 4H_2O \quad (4)$$

From eqn. 4, the potential for the etching process can be described by the following expression:

$$\Delta E = \Delta E^0 - \frac{0.059}{4}\left\{\log\frac{[SiF_6^{2-}]}{[H_2O_2]^2[H^+]^4[F^-]^6}\right\} \quad (5)$$

It is evident from the expression that with increase in H_2O_2 concentration, the potential for the etching process increases. This shows that thermodynamically, the reaction for etching is more favourable for the growth of SiNWs. So the height of the SiNWs depends mostly on oxidant concentration (H_2O_2). However, the oxidant concentration cannot be increased infinitely. For instance, Liu *et al.* [25] observed that the variation of H_2O_2 concentration to very high values leads to change in the morphology from polished nanowires to porous structured nanowires. Similarly, Moumni & Jaballah [24] reported that the variation of H_2O_2 to high concentrations significantly influence the etching rate Si wafer. They have observed a nonlinear height dependence on H_2O_2 concentration with the attenuation of height of the nanowires at high concentration. This can be

understood based on the fact that, although the H_2O_2 concentration increases to high values, the etching solution may not have enough HF to dissolve the formed SiO_2 at the same rate of etching. Therefore, it is preferable to select a suitable concentration of etching solution to produce good quality SiNWs. On considering these facts, in this work, SiNWs were fabricated by selecting a suitable concentration of the etchant where the variation of etching parameter has only changed the height of nanowalls. The agglomeration of SiNWs formed at high H_2O_2 concentration can also be explained based on the fact that the surface tension forces acting on SiNWs during the drying process [27], exceeds the elastic deformation force of SiNWs for long nanowalls.

Reflectivity: Fig. 4 shows the reflectance and absorbance spectra of fabricated SiNWs, in the wavelength range of 300-1100 nm. For comparison, the reflectance and absorbance spectra of planar Si wafer are also depicted in Fig. 4. The absorbance (A) of the samples can be calculated from the reflectance (R) data using the relation, A = (100-R) %, because the present Si wafer is an opaque material with almost zero transmittance. It is observed from Fig. 4a that the reflectance was reduced tremendously when SiNWs are formed atop Si wafer. Moreover, as shown in the inset of Fig. 4a, the reflectance behaviour is wavelength dependent as well as H_2O_2 concentration. So, it is convenient to investigate the reflectance in the following regions (i) short (300-750 nm) and long (750-1100 nm) wavelength regions; and (ii) low (0.2-0.4 M) and high (0.6-1 M) H_2O_2 concentrations. The SiNWs prepared at low H_2O_2 concentration (0.2 and 0.4 M) show comparatively low and high reflectance at short (300-750 nm) and long (750-1100 nm) wavelength regions, respectively and *vice-versa* for sample prepared at high H_2O_2 concentrations (0.6, 0.8 and 1.0 M). With increase in H_2O_2 concentration, the reflectance value decreases gradually in the long wavelength region (750-1100 nm) whereas in short wavelength region (300-750 nm), the reflectance first decreases with increase in H_2O_2 concentration from 0.2 to 0.4 M (low H_2O_2 concentration region) and then increases gradually with increase in H_2O_2 concentration from 0.6 to 1 M (high H_2O_2 concentration region). Such extremely low and peculiar wavelength dependent reflectance was previously reported and pointed out that the peculiar wavelength dependence of reflectance is ascribed to be due to the agglomeration/bunching of SiNWs [28].

In order to make a comparison among the SiNWs prepared at different H_2O_2 concentration for solar cell application, it is important to estimate the following factors; (i) solar weighted reflectance (R_{SW}) from the reflectance spectra and (ii) ultimate efficiency (η) from the absorbance spectra. These are represented by the following expressions [29,30]:

$$R_{SW} = \frac{\int_{300\ nm}^{\lambda_g} R(\lambda) N_{photon}(\lambda) d\lambda}{\int_{300\ nm}^{\lambda_g} N_{photon}(\lambda) d\lambda} \quad (6)$$

$$\eta = \frac{\int_{300\ nm}^{\lambda_g} N_{photon}(\lambda) A(\lambda) \frac{\lambda}{\lambda_g} d\lambda}{\int_{300\ nm}^{4000\ nm} N_{photon}(\lambda) d\lambda} \quad (7)$$

where $R(\lambda)$ and $A(\lambda)$ are the spectral reflectance and absorbance of the SiNWs, respectively; $N_{photon}(\lambda)$ is the photon number of AM 1.5 G per unit area per unit wavelength, λ_g is the wavelength corresponding to band gap of Si ($\lambda_g \approx 1100$

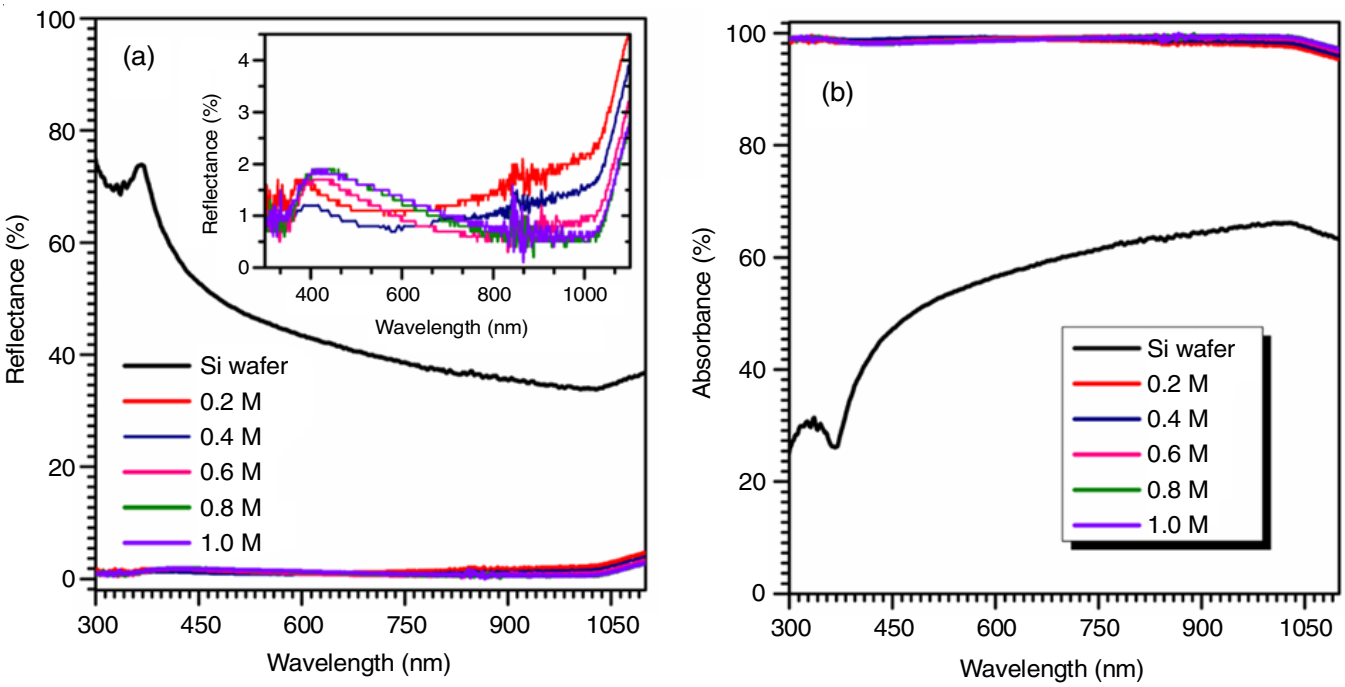

Fig. 4. (a) Reflectance curves of SiNWs prepared at various H_2O_2 concentrations in the wavelength range of 300-1100 nm. For a reference, the reflectance curve of planar Si wafer is also depicted. The inset displays an enlarged view of the reflectance spectra of SiNWs. (b) Absorbance curves of SiNWs prepared at various H_2O_2 concentrations in the wavelength range of 300-1100 nm. The absorbance curve of planar Si wafer is also depicted in the figure

nm). For the calculation of ultimate efficiency, it is assumed that each photon absorbed produces one electron-hole pair and carrier recombination processes are absent.

The estimated values of R_{SW} and η of the SiNWs are summarized in Table-1, which clearly indicate extremely low R_{SW} value compared to that of planar Si wafer (43.91%). The R_{SW} value first decreases and research to minimum (for 0.4 and 0.6 M H_2O_2) and then again increases with H_2O_2 concentration. The minimum R_{SW} value obtained is mainly due to their comparatively low reflectance value in both short (300-750 nm) and long (750-1100 nm) wavelength regions as well as the spectral dependence of the AM 1.5 G solar spectrum. Similarly, the η value is very high for SiNWs compared to that of planar Si wafer (28.59%). It increases with H_2O_2 concentration, reaches maximum and then decreases. However, it is important to observe that the η value for SiNWs prepared at 0.8 and 1 M H_2O_2 concentration is higher than that for SiNWs prepared at 0.4 M H_2O_2 concentration, although R_{SW} value for SiNWs prepared at 0.8 and 1 M H_2O_2 concentration is higher than that of SiNWs prepared at 0.4 M H_2O_2 concentration.

TABLE-1
ESTIMATED VALUE OF SOLAR WEIGHTED REFLECTANCE (R_{SW}) AND ULTIMATE EFFICIENCY (η) FOR PLANAR Si WAFER AND SiNWs PREPARED AT VARIOUS H_2O_2 CONCENTRATIONS

Sample	Solar weighted-reflectance (R_{SW}, %)	Ultimate efficiency (η, %)
0 M (Si wafer)	43.91	28.59
0.2 M	1.46	48.21
0.4 M	1.08	48.40
0.6 M	1.06	48.48
0.8 M	1.17	48.45
1.0 M	1.23	48.42

This is mainly due to the low reflectance value of SiNWs prepared at 0.8 and 1 M H_2O_2 concentration, compared to that of SiNWs prepared at 0.4 M H_2O_2 concentration at long wavelength region (750-1100 nm) as well as the band gap value of Si at ~1100 nm (eqn. 7).

Wettability studies: The wetting behaviour of the fabricated SiNWs was investigated by measuring the water contact angle (WCA). For comparison, the WCA value obtained for planar Si wafer is also depicted. Fig. 5a shows the WCA value as a function of H_2O_2 concentration. The photographs of water droplets on a planar Si wafer and SiNWs prepared at 0.2, 0.4, 0.6, 0.8 and 1.0 M H_2O_2 concentrations are given in Fig. 5b-g, respectively.

The WCA value obtained for planar Si wafer and SiNWs prepared at 0.2, 0.4, 0.6, 0.8, 1 M H_2O_2 concentration are 73 ± 1º, 139 ± 1º, 140 ± 1º, 130 ± 1º, 84 ± 1º, 63 ± 2º, respectively. Generally, if the water contact angle is less than 90 ºC, the solid surface is considered as hydrophilic and if the water contact angle is greater than 90 ºC, the solid surface is considered as hydrophobic. If so, planar Si wafer and SiNWs prepared above 0.6 M H_2O_2 concentration exhibits hydrophilic behaviour and SiNWs prepared below 0.6 M H_2O_2 concentration exhibits hydrophobic behaviour. Based on these experimental data (Fig. 5a), it has been shown that the hydrophilic planar Si surface transforms to hydrophobic behaviour when patterned with the SiNWs. The hydrophobic behaviour continues for SiNWs prepared up to 0.6 M H_2O_2 concentration. When the concentration of H_2O_2 is further increased, the hydrophilic behaviour reappears. The wetting behaviour SiNWs prepared at higher concentration of H_2O_2 can be ascribed to the vertical and high agglomeration of SiNWs. prepared at low and very high H_2O_2 concentration, respectively [28].

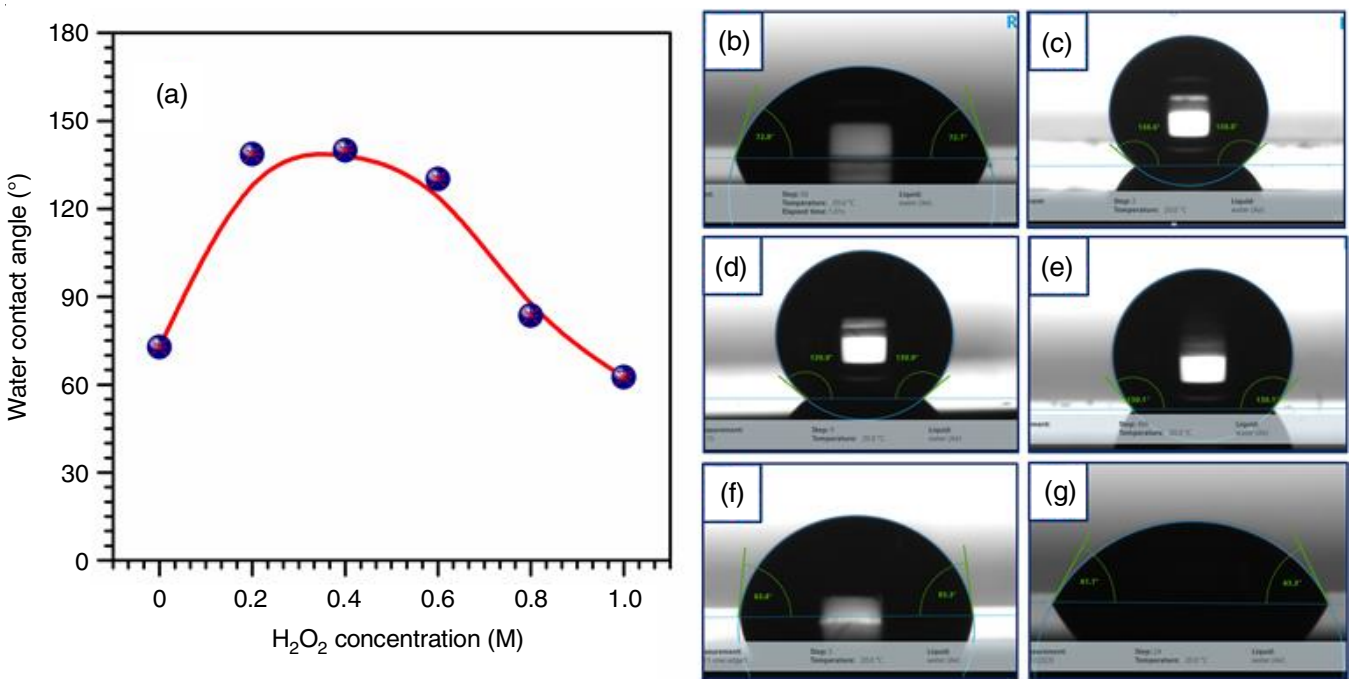

Fig. 5. (a) A plot of water contact angle (WCA) as a function of H_2O_2 concentration. The 0 M denotes the planar Si wafer. (b-g) Display the photographs of water droplet on a planar Si wafer and SiNWs prepared at 0.2, 0.4, 0.6, 0.8 and 1 M H_2O_2, respectively

Conclusion

The single crystalline silicon nanowalls were fabricated atop the Si wafer by a simple and low cost metal assisted chemical etching method. The effect of etchant solution concentration (H_2O_2 concentration) on the morphology, reflectivity and wettability parameters was investigated. It is revealed from the reflectance/absorbance and wetting studies of Si nanowalls prepared at different H_2O_2 concentration, that the Si nanowalls prepared at 0.4 H_2O_2 concentration exhibit comparatively low solar weighed-reflectance, $R_{SW} = 1.08\%$ (high value of ultimate efficiency, $\eta = 48.40\%$) and the highest value of water contact angle, WCA = 140 ± 1° and is the optimal sample for solar cell applications for increasing its efficiency as well as lifetime due to the self-cleaning nature of hydrophobicity.

ACKNOWLEDGEMENTS

The authors thank P.K. Ajikumar and S. Amirthapandian of Indira Gandhi Centre for Atomic Energy for SEM and TEM analyses. One of the authors, RNV thanks Aarupadai Veedu Institute of Technology, Vinayaka Mission's Research Foundation (DU), Chennai, India for the constant research support and encouragement.

CONFLICT OF INTEREST

The authors declare that there is no conflict of interests regarding the publication of this article.

REFERENCES

1. Z. Zhuang, Q. Peng and Y. Li, *Chem. Soc. Rev.*, **40**, 5492 (2011); https://doi.org/10.1039/C1CS15095B
2. F.J. Wendisch, M. Rey, N. Vogel and G.R. Bourret, *Chem. Mater.*, **32**, 9425 (2020); https://doi.org/10.1021/acs.chemmater.0c03593
3. R. Smith, W. Duan, J. Quarterman, A. Morris, C. Collie, M. Black, F. Toor and A.K. Salem, *Adv. Mater. Technol.*, **4**, 1800349 (2019); https://doi.org/10.1002/admt.201800349
4. A.A. Leonardi, M.J.L. Faro and A. Irrera, *Nanomaterials*, **11**, 383 (2021); https://doi.org/10.3390/nano11020383
5. H. Alhmoud, D. Brodoceanu, R. Elnathan, T. Kraus and N.H. Voelcker, *Prog. Mater. Sci.*, **116**, 100636 (2021); https://doi.org/10.1016/j.pmatsci.2019.100636
6. A. Matsumoto, M. Eguchi, K. Iwamoto, Y. Shimada, K. Furukawa, H. Son and S. Yae, *RSC Adv.*, **10**, 253 (2020); https://doi.org/10.1039/C9RA08728A
7. A.K. Behera, C. Lakshmanan, R. Viswanath, C. Poddar and T. Mathews, *Bull. Mater. Sci.*, **43**, 291 (2020); https://doi.org/10.1007/s12034-020-02272-7
8. K. Kim, J.K. Lee, S.J. Han and S. Lee, *Appl. Sci.*, **10**, 1146 (2020); https://doi.org/10.3390/app10031146
9. M.H. Kafshgari, N.H. Voelcker and F.J. Harding, *Nanomedicine*, **10**, 2553 (2015); https://doi.org/10.2217/nnm.15.91
10. A.K. Behera, R. Viswanath, C. Lakshmanan, K. Madapu, M. Kamruddin and T. Mathews, *Micropor. Mesopor. Mater.*, **273**, 99 (2019); https://doi.org/10.1016/j.micromeso.2018.06.052
11. A.A. Leonardi, M.J. Lo Faro and A. Irrera, *Nanomaterials*, **10**, 966 (2020); https://doi.org/10.3390/nano10050966
12. A.K. Behera, R. Viswanath, C. Lakshmanan, S. Polaki, R. Sarguna and T. Mathews, *AIP Conf. Proc.*, **1942**, 050062 (2018); https://doi.org/10.1063/1.5028693
13. M.Y. Arafat, M.A. Islam, A.W.B. Mahmood, F. Abdullah, M. Nur-E-Alam, T.S. Kiong and N. Amin, *Sustainability*, **13**, 10766 (2021); https://doi.org/10.3390/su131910766
14. A.K. Behera, R. Viswanath, C. Lakshmanan, T. Mathews and M. Kamruddin, *Nano-Structures Nano-Objects*, **21**, 100424 (2020); https://doi.org/10.1016/j.nanoso.2020.100424
15. R. Venkatesan, J. Mayandi, J.M. Pearce and V. Venkatachalapathy, *J. Mater. Sci. Mater. Electron.*, **30**, 8676 (2019); https://doi.org/10.1007/s10854-019-01191-6
16. A.M. Gouda, N.K. Allam and M.A. Swillam, *RSC Adv.*, **7**, 26974 (2017); https://doi.org/10.1039/C7RA03568C
17. F. Toor, J.B. Miller, L.M. Davidson, W. Duan, M.P. Jura, J. Yim, J. Forziati and M.R. Black, *Nanoscale*, **8**, 15448 (2016); https://doi.org/10.1039/C6NR04506E
18. Z. Fan, D. Cui, Z. Zhang, Z. Zhao, H. Chen, Y. Fan, P. Li, Z. Zhang, C. Xue and S. Yan, *Nanomaterials*, **11**, 41 (2020); https://doi.org/10.3390/nano11010041
19. S.R. Marthi, S. Sekhri and N. Ravindra, *J. Miner. Met. Mater. Soc.*, **67**, 2154 (2015); https://doi.org/10.1007/s11837-015-1527-0
20. H.D. Omar, M.R. Hashim and M.Z. Pakhuruddin, *Opt. Laser Technol.*, **136**, 106765 (2021); https://doi.org/10.1016/j.optlastec.2020.106765
21. J.Y.-H. Chai, B.T. Wong and S. Juodkazis, *Mater. Today Energy*, **18**, 100539 (2020); https://doi.org/10.1016/j.mtener.2020.100539
22. A. Gouda, M. Elsayed, A. Khalifa, Y. Ismail and M.A. Swillam, *Opt. Lett.*, **41**, 3575 (2016); https://doi.org/10.1364/OL.41.003575
23. L. Rosales and J.W. González, *Nanoscale Res. Lett.*, **8**, 1 (2013); https://doi.org/10.1186/1556-276X-8-1
24. B. Moumni and A.B. Jaballah, *Appl. Surf. Sci.*, **425**, 1 (2017); https://doi.org/10.1016/j.apsusc.2017.06.110
25. Y. Liu, G. Ji, J. Wang, X. Liang, Z. Zuo and Y. Shi, *Nanoscale Res. Lett.*, **7**, 663 (2012); https://doi.org/10.1186/1556-276X-7-663
26. M. Naffeti, P.A. Postigo, R. Chtourou and M.A. Zaïbi, *Nanomaterials*, **10**, 404 (2020); https://doi.org/10.3390/nano10030404
27. A.S. Togonal, L. He, P. Roca i Cabarrocas and Rusli, *Langmuir*, **30**, 10290 (2014); https://doi.org/10.1021/la501768f
28. A.K. Behera, R. Viswanath, N. Sharma, P. Ajikumar, S.T. Sundari and T. Mathews, *Nano-Structures Nano-Objects*, **29**, 100833 (2022); https://doi.org/10.1016/j.nanoso.2021.100833
29. H. Sai, Y. Kanamori, K. Arafune, Y. Ohshita and M. Yamaguchi, *Prog. Photovolt. Res. Appl.*, **15**, 415 (2007); https://doi.org/10.1002/pip.754
30. F.-Q. Zhang, K.-Q. Peng, R.-N. Sun, Y. Hu and S.-T. Lee, *Nanotechnology*, **26**, 375401 (2015); https://doi.org/10.1088/0957-4484/26/37/375401